where $b = 1.7e^{(E_{mn}-E_c)/kT}$. Integrating (A7) yields

$$D = \frac{kT\nu}{1.7} e^{(E_{mn}-E_c)/kT}\left[\tan^{-1}(1.7e^{(E_{mn}-E_v)/kT}) - \tan^{-1}(1.7e^{(E_{mn}-E_c)/kT})\right]. \quad \text{(A8)}$$

Generally speaking, $(E_{mn}-E_v)/kT$, $(E_c-E_{mn})/kT \gg 1$, so that the contents of the square brackets evaluate to approximately $\frac{1}{2}\pi$, hence (A8) reduces to

$$D = 1.2kT\nu e^{(E_{mn}-E_c)/kT} \quad \text{(A9)}$$

or, by using (8),

$$D = 1.2\beta(E_c - E_{mn})/T. \quad \text{(A10)}$$

*Supported in part by National Research Council and Defense Research Board of Canada.

†Now with Uniroyal Research Center, Guelph, Ontario, Canada.

[1]J. J. Randall and M. H. F. Wilkens, Proc. Roy. Soc. A184, 366 (1945); A184, 390 (1945).
[2]K. H. Nicholas and J. Woods, Brit. J. Appl. Phys. 15, 783 (1964).
[3]G. A. Dussel and R. H. Bube, Phys. Rev. 155, 764 (1967).
[4]R. Chen, J. Appl. Phys. 40, 570 (1969).
[5]I. J. Saunders, J. Phys. 2, 2181 (1969).
[6]P. S. Pickard and M. V. Davis, J. Appl. Phys. 41, 2636 (1970).
[7]P. Kelly and P. Braunlich, Phys. Rev. B 1, 1587 (1970).
[8]J. G. Simmons and G. W. Taylor, Phys. Rev. B 4, 502 (1971).
[9]J. G. Simmons and G. W. Taylor, Phys. Rev. B 5, 1619 (1972).
[10]J. G. Simmons and M. C. Tam, preceding paper, Phys. Rev. B 7, 3706 (1973).
[11]J. G. Simmons and G. W. Taylor, Phys. Rev. B (to be published).
[12]J. G. Simmons and G. W. Taylor, Phys. Rev. B (to be published).
[13]J. G. Simmons and G. S. Nadkarni, Phys. Rev. B (to be published).

PHYSICAL REVIEW B VOLUME 7, NUMBER 8 15 APRIL 1973

Isothermal-Dielectric-Relaxation Currents in Thin-Film Al-CeF_3-Al Samples*

G. S. Nadkarni† and J. G. Simmons
Electrical Engineering Department, University of Toronto, Toronto, Canada
(Received 2 June 1972)

A new technique based on isothermal-dielectric-relaxation currents (IDRC) had been successfully used to study the defect properties of thin-film Al-CeF_3-Al samples. The IDRC technique consists of applying a step voltage to the sample to induce a non-steady state and then measuring the non-steady-state current as a function of time as the system decays to the steady state. It is found that at low temperatures ($T < 250$ °K), the displacement charge Q_d circulating the external circuit is associated with the geometrical capacitance. Thus, it is inversely proportional to the thickness of the sample and linearly dependent on the voltage. At higher temperatures ($T > 280$ °K) a pronounced dielectric-relaxation current flows through the insulator. The displacement charge Q_r associated with the relaxation current is found to be 20–40 times the magnitude of Q_d and *independent* of the thickness of the insulator at low voltages, indicating the existence of Schottky barriers at the electrode insulator and, thus, that the conduction process is electrode limited. At higher voltages $V \gtrsim 4$ V, Q_r saturates showing that the conduction process is bulk limited. From the Q_r-V characteristic, the trapping density is found to be 6×10^{19} cm^{-3}. The It-$\log_{10}t$ characteristic is shown to manifest a pronounced peak. From this characteristic, it is determined that the occupied trap levels are contained in a band of energy of width approximately 0.02 eV, which is centered about an energy 0.63 ± 0.03 eV below the bottom of the conduction band. The results are shown to be consistent with IDRC theory and previous stimulated-dielectric-relaxation-current studies on the same samples.

I. INTRODUCTION

In recent papers it was shown, on theoretical grounds, that Schottky barriers can exist at the metal-insulator interface of metal-insulator-metal (MIM) systems when the insulator is defect in nature.[1–3] ac and dc measurements[4–8] on MoO_3, SiO, and CeF_3 films have confirmed the existence of these barriers. Stimulated-dielectric-relaxation-current[7,8] (SDRC) measurements on a wide variety of materials (MoO_3, SiO, CeF_3, $BaTiO_3$, Al_2O_3, and many semiconducting glasses) have also shown Schottky barriers to exist at the electrode-insulator/semiconductor interfaces.

In this paper we will be concerned with a new technique of determining information concerning the energy diagram and the trap parameters of MIM systems containing interfacial Schottky barriers. This technique involves the use of isothermal-dielectric-relaxation currents (IDRC) that flow in the MIM systems as they relax from the non-steady-state to the steady state.[9] Here we will study specifically Al-CeF_3-Al samples, which we have already investigated thoroughly using SDRC techniques.[8] As we will show, the analysis of IDRC studies confirm the results obtained from the SDRC measurements.

II. EXPERIMENTAL TECHNIQUES

A. Sample Fabrication

The Al-CeF_3-Al samples used here are those used in earlier SDRC studies and the reader is referred to Ref. 8 for details of their preparation. The thickness d of the CeF_3 films ranged in steps, from 1800 to 4900 Å; the area A of the samples is 0.1 cm^2; and the dielectric constant K is 10.

B. IDRC Measurements

The I-t measurements were made by applying a step voltage V to the sample at time $t=0$. The sample current was measured using a Keithley 610C electrometer, which has a response time of milliseconds, and the temperature of the sample was monitored with a thermocouple. The current I was plotted continuously and automatically as a function of time t by feeding the electrometer output either to the y axis of a Moseley 7001 AM

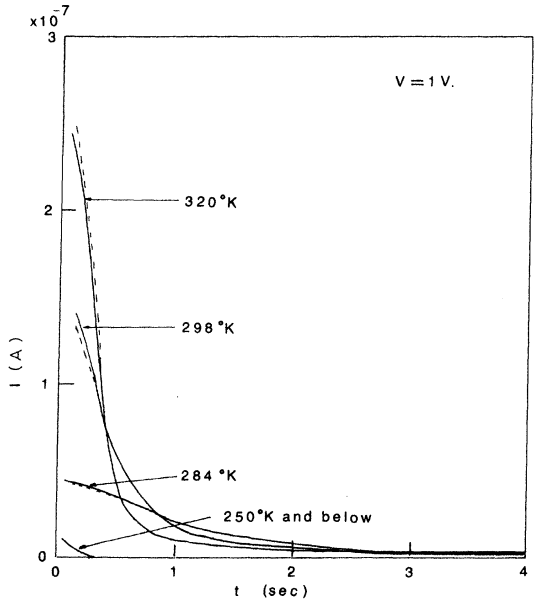

FIG. 1. I-t characteristics as a function of temperature for a step voltage of $V=1.0$ V.

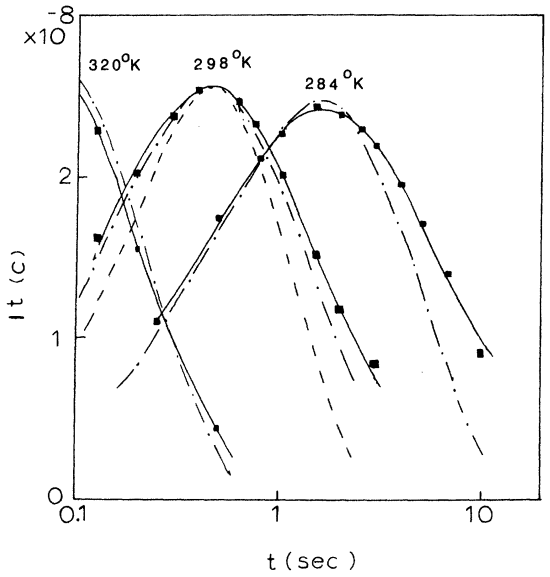

FIG. 2. I-t characteristics in Fig. 1 replotted as It vs $\log_{10}t$ (full curve). The dotted and chain-dotted curve in this figure are the theoretical It-vs-$\log_{10}t$ characteristics for discrete traps and distributed traps, respectively.

X-Y recorder, the X axis of which was driven by the time base of the recorder, for relatively slowly decaying current, or to a storage oscilloscope when the decay was fast. In order to minimize deleterious ambient effects, the measurements were made under vacuum ($\simeq 10^{-3}$ Torr).

III. EXPERIMENTAL RESULTS

A. I-t Characteristics at Various Temperatures

Figure 1 shows the I-t characteristics for the sample at different temperatures for an applied voltage bias of 1.0 V. Below about 250 °K the I-t characteristics are virtually independent of temperature. However, above 250 °K there is a dramatic shift in the current to higher levels. At 320 °K the maximum current has increased by about 20 times but the area under the curves, when extended to very long times, was constant and independent of the thickness of the CeF_3 film. Furthermore, the rate of decay of current was faster the higher the temperature.

Figure 2 shows the high-temperature data of Fig. 1 replotted as It-$\log_{10}t$ characteristics. The interesting feature of these curves is that they show a pronounced peak, the maxima of which shift to higher values of $\log_{10}t$ as the temperature is decreased. The shape and size of these peaks are virtually independent of temperature.

B. I-t Characteristics for Various Voltage Biases

Figure 3 illustrates the I-t characteristics for various voltage steps measured at 320 °K for vari-

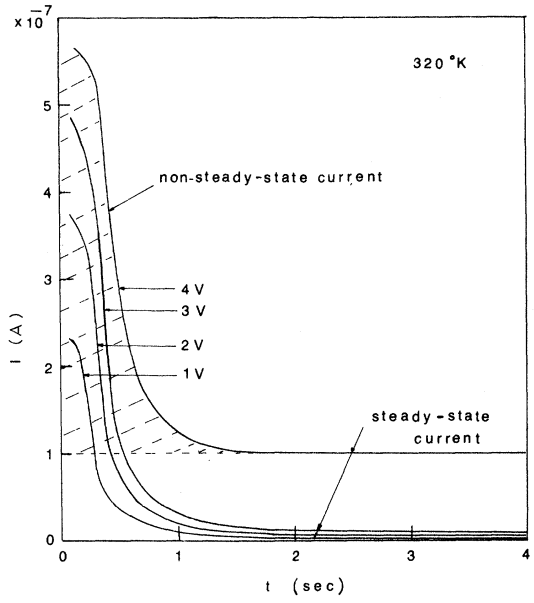

FIG. 3. *I-t* characteristics at 320 °K for various step-voltage biases.

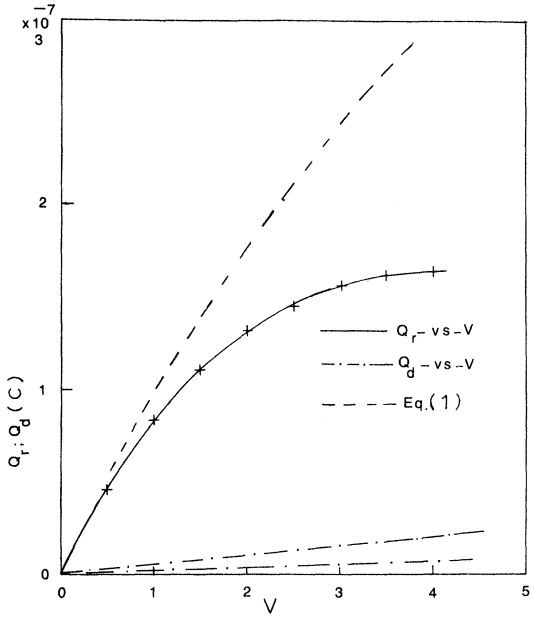

FIG. 4. Full curve is the experimental Q_r-vs-V characteristic. The dotted line is the theoretical curve (1). Chain-dotted line is the Q_d-vs-V characteristic.

ous voltage biases. For $t > t_r$, the relaxation time, the sample is in the non-steady-state, and for $t < t_r$ it is in the steady state. The non-steady-state current is always greater than the steady-state current, and both currents shift to higher levels with increasing voltage bias.

The charge Q_r associated with the area under the non-steady-state portion (e.g., hatched portion of the 4-V curve) of the characteristics is plotted as a function of voltage in Fig. 4. Initially it is seen that Q_r increases with voltage bias, but eventually saturates at higher voltages. Also illustrated in Fig. 4 is the displacement charge Q_d associated with the geometrical capacitance C_g, i.e., $Q_d = VC_g$, for the thinnest ($d = 1800$ Å) and thickest ($d = 4900$ Å) samples used.

Figure 5 shows the *I-t* characteristics for a

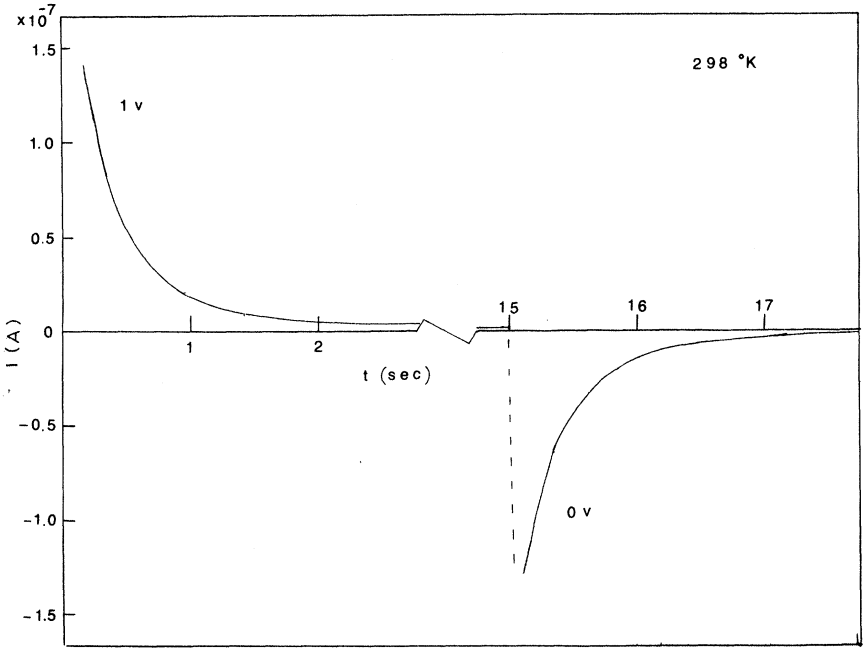

FIG. 5. *I-t* characteristics for step ($t = 0$ sec–$t = 15$ sec) voltage 1.0 V and when the step voltage is removed ($t \gtrsim 15$ sec).

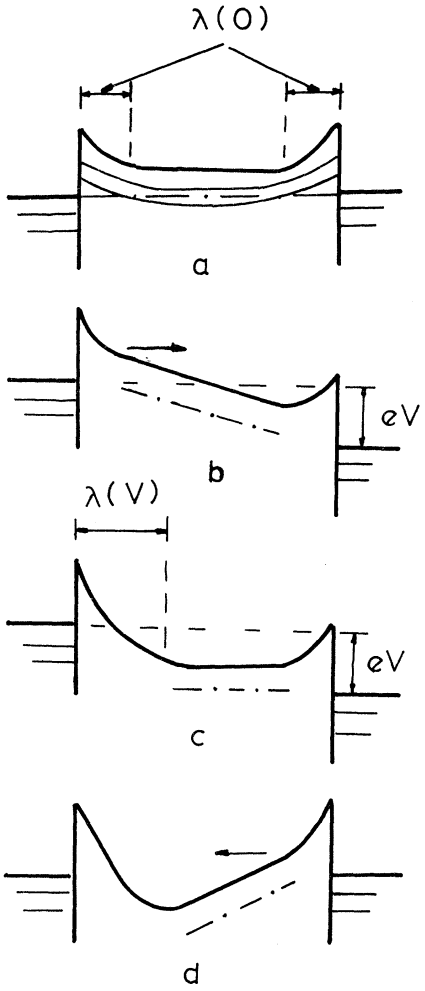

FIG. 6. Energy diagrams for an MIM system containing Schottky barriers: (a) in equilibrium; (b) immediately after a step voltage V is applied; (c) in the steady state, with a voltage V applied; and (d) immediately after the voltage is removed.

voltage step $V = 1.0$ V ($t = 0$–15 sec), and after the voltage pulse has been removed ($t > 15$ sec). It is seen that during the period after which the pulse is removed, a *negative* current (that is, it flowed in the opposite direction to that of the initial current) flows in the system.

All the above-mentioned data were essentially independent of the polarity of the voltage bias.

IV. DISCUSSION

A. Evidence for the Existence of Schottky Barriers

There are two striking pieces of evidence that suggest that Schottky barriers exist at the interface. First, the non-steady-state relaxation charge Q_r above $T \simeq 250$ °K is found to be *independent* of the insulator thickness, suggesting that the phenomenon is associated with the contacts. Furthermore, the charge released during the relaxation process is much greater than can be accounted for from geometrical capacitance considerations. This is clearly evident by reference to Fig. 4. In this diagram it is seen that the observed charge Q_r-vs-voltage characteristic (full curve) is not linear with voltage—in fact it saturates for voltages in excess of 4 V—and is typically 20 to 40 times greater than the geometrical charge Q_d-vs-voltage characteristic (chain-dotted curve).

We note that the above observations cannot be accounted for in terms of *injected* space-charge capacitance, which is thickness dependent and at best can only be *twice* the geometric capacitance.

We now proceed to explain the rest of the experimental data assuming that Schottky barriers exist at the interface.

B. Schottky Effects

Figure 6(a) illustrates an MIM system containing Schottky barriers under zero-voltage bias. Immediately after a voltage V is applied to the electrodes, it is uniformly distributed throughout the insulator [Fig. 6(b)], in which case the system is in the non-steady state. (The application of the voltage bias causes a displacement current $Q_d = C_g V$ to flow momentarily in the external circuit.) Ultimately, the system will decay to the steady state, as illustrated by the energy diagram in Fig. 6(c). The time t_r taken for the system to reach the steady state is a function of the trap depth and the temperature. This time is the dielectric relaxation time of the system.[9]

In the steady state for low applied voltages, the majority $(V - \Delta V)$ of the applied voltage is dropped across the reverse-biased (cathodic) Schottky barrier, the remaining fraction ΔV being dropped across the interior and the forward-biased (anodic) Schottky barrier [Fig. 6(c)] which is just sufficient to ensure current continuity throughout the system. Clearly, as a result of the system relaxing from the non-steady state to the steady state, the cathodic depletion region has grown from $\lambda(0)$ to $\lambda(V)$ in size, emptying the traps contained therein. Consequently, the insulator now contains an excess positive charge Q_r given by

$$Q_r = qN_t[\lambda(V) - \lambda(0)] \,. \tag{1}$$

For a spacially uniform trap density N_t, $\lambda(V)$ is given by[10]

$$\lambda(V) = \left(\frac{2K\epsilon_0}{qN_t}\right)^{1/2} [\phi_m - \phi_i + q(V - \Delta V)]^{1/2} \,, \tag{2}$$

where ϕ_m and ϕ_i are the work functions of the cathode and insulator, respectively, ϵ_0 is the permittivity of free space, and q is the unit of electronic charge. Clearly, Q_r may also be expressed

in the form

$$Q_r \simeq C_\lambda V , \tag{3}$$

where C_λ [$=KA\epsilon_0/\lambda(V)$] is the capacitance of the cathodic depletion region. Thus,

$$\frac{Q_r}{Q_d} \simeq \frac{C_\lambda V}{C_g V} \simeq \frac{d}{\lambda} \gg 1 \tag{4}$$

as observed.

C. Effect of Temperature

When the energy E_t^* of the uppermost filled trap satisfies the inequality

$$e_n(E_t^*) = \nu e^{(E_t^* - E_c)/kT} \ll 1 , \tag{5}$$

where e_n is the emission probability of the trap and ν is the attempt-to-escape frequency of the traps, the system will remain in the non-steady state indefinitely. Thus, the charge that circulates the external circuit on application of a step voltage is simply the relaxation charge Q_d associated with the geometrical capacitance of the system. As such, it is inversely proportional to the thickness of the insulator, essentially independent of temperature and relatively small, and is the charge associated with the area under the I-t characteristics for $T < 250$ °K shown in Fig. 1 (see also chain-dotted lines in Fig. 4).

When the inequality

$$e_n(E_t^*) > 1 \tag{6}$$

prevails, the system relaxes from the non-steady state to the steady state in a relatively short period of time. In this case, the charge circulating the external circuit is that associated with the charge Q_r released from the originally occupied traps located in the cathodic depletion region and, as such, is *independent* of the insulator thickness and the temperature. Also, the rate of decay of current is greater the higher the temperature.[9] It will be evident that these remarks qualitatively explain the nature of the I-t curves for $t > 250$ °K shown in Fig. 1.

Clearly, the current is proportional to the rate that electrons are swept out of the depletion region. Also, since the number of free holes in the depletion region of a Schottky barrier in an *insulator* is extremely *small*, the probability of an electron recombining with a free hole is extremely small. Hence, an electron escaping from a trap in the depletion region will be swept out of the depletion region (active region[11]). Thus, the experimental data are ideally amenable to analyses by the high-field isothermal current theory contained in Paper I.[11] Consequently, if the trap level is relatively discrete,[10] the I-t characteristic is given by[11]

$$I \simeq Be_n(\bar{E}_t)e^{-e_n(\bar{E}_t)t} , \tag{7}$$

where $\bar{E}_t$ is the average trap depth of the trap levels, and B is a constant for a given voltage bias. In Fig. 1, (7) is shown plotted for $T = 284$, 298, and 320 °K, and $E_c - E_t = 0.63$ eV. It is seen that the correlation between theory and experiment is very good.

A much more powerful and sensitive way[11] of illustrating the isothermal characteristics is by plotting the data in the form It-vs $\log_{10}t$, as shown in Fig. 2. This type of characteristic has the advantage in that it yields *directly* information on the trap parameters. For example, if the traps are distributed throughout the band gap, the characteristic is a direct image of trapping distribution in the band gap. Thus, one can immediately determine the trap density and distribution. Alternatively, if the trap level is relatively discrete, the characteristic will determine the degree of discreteness of the trap level and yield directly the trap depth. Now, from previous SDRC measurements, we know that the trap level is relatively discrete, and since the depletion region contains only electron-emitting traps, the It-$\log_{10}t$ characteristic for discrete traps is given by[10,11]

$$It = Bte_n(\bar{E}_t)e^{-e_n(\bar{E}_t)t} . \tag{8}$$

This characteristic has a maximum that occurs at $t = t_m$, which is related to the trap depth $\bar{E}_t$ by the equation

$$E_c - \bar{E}_t = kT \ln(\nu t_m) . \tag{9}$$

Let us analyze the characteristics shown in Fig. 2 (assuming there are the result of discrete traps) using (8) and (9). From Fig. 2 we find that t_m (298 °K = 1.6 sec and t_m (284 °K) = 0.48 sec. Substituting these values into (9), we obtain two simultaneous equations which yield

$$\nu = (1 \pm 5) \times 10^{11} \text{ sec}^{-1}$$

and

$$E_c - E_t = 0.63 \pm 0.03 \text{ eV} . \tag{10}$$

(These values of the parameters are in very good agreement with those calculated from SDRC measurements.[8]) The dotted line in Fig. 2 is the theoretical curve computed using (8) and (10) and $B = 7.5 \times 10^{-8}$. Although the correlation between the theoretical and experimental curves is quite good, the fact that the experimental curve is wider than the theoretical curve indicates that the trap levels are, in fact, not located in a discrete energy level. Also the fact that the two experimental peaks are not of the same height is further indication that the trap levels are not discrete. In fact, we know from SDRC measurements[8] that the spread in energy of the trap levels is about 0.02 eV. Assuming this value[13] to be applicable for the case in hand, we can construct an approxi-

mate It-$\log_{10} t$ characteristic that takes into account this energy spread, in the following manner. Using (8) we construct two curves using $E_c - E_t = 0.64$ eV (i.e., $0.63 + 0.01$ eV) and 0.62 eV (i.e., $0.63 - 0.01$ eV) and then sum the two characteristics to obtain the required characteristic. The result of this procedure is shown by the chain-dotted line in Fig. 2. It will be observed that the correlation between the experimental and the theoretical curves is quite good. We note here that the maximum value of the theoretical curve decreases with decreasing temperature, as do the experimental curves, which is a characteristic feature of a nondiscrete trapping level. Thus, we conclude that the occupied trap levels are spread in energy over about 0.02 eV, which is in accordance with the value obtained from SDRC studies.

D. Effect of Voltage Bias

The dotted line in Fig. 4 is the theoretical Q_r-vs-V characteristic (1). The value of N_t used in (1) to obtain the correlation between the theoretical and experimental curves at the lower-voltage values was approximately 5×10^{19} cm^{-3}, which is in reasonable agreement with that (3×10^{20} cm^{-3}) obtained from SDRC measurements.[8] The disparity between the two curves at higher voltages, and the saturation of the experimental curve are explained as follows. The theoretical characteristic (1) was derived on the basis of a cathodic contact that is blocking at all values of V. However, it has been shown that in MIM systems containing Schottky barriers,[3] above a certain voltage V_t (the transition voltage), the conduction process undergoes an electrode-limited–to–bulk-limited transition. What this means, as far as we are concerned, is that for voltages above V_t, a decreasing fraction of the applied voltage in excess of V_t appears across the cathodic depletion region, with the result that Q_r grows less rapidly with increasing voltage than it would if the contact were perfectly blocking. Above 4 V the characteristic saturates, which is an indication that the conduction process is essentially bulk limited in this range. Similar conclusions were deduced from SDRC measurements.

The negative-current characteristic in Fig. 5 can be explained with references to Figs. 6(c) and (d). Figures 6(c) and 6(d) correspond to the energy diagrams for the system just before and immediately after the electrodes have been short circuited. Figure 6(d) clearly illustrates a nonsteady-state situation, and the system decays to the equilibrium state indicated by the energy diagram in Fig. 6(a). It will be apparent from the slope of the conduction band in the interior of the insulator in Fig. 6(d) that the electrons must flow towards the original cathodic depletion region in order to neutralize the excess positive charge therein. Hence, the direction of flow of the associated conventional current is opposite to that of the original relaxation current. Furthermore, the amount of electronic charge required to annihilate the excess positive charge is approximately equal to Q_r, which is the reason that the areas under the positive-current and negative-current I-t characteristic are essentially equal (Fig. 5).

V. CONCLUSIONS

We have shown that the isothermal dielectric relaxation characteristics provide a powerful means of determining the energy-band diagram of the system and the defect parameters of the insulator. In particular, we have shown that Schottky barriers exist at the electrode-insulator interface, and that the insulator contains a band of occupied trapping levels approximately 0.02 eV wide and centered about an energy 0.63 ($\pm$0.03) eV below the bottom of the conduction band. The density of the traps was estimated to be 6×10^{19} cm^{-3}.

At low voltages all the results were found to be essentially independent of the thickness of the insulator, indicating that the conduction process is electrode limited. However, at higher voltages ($V > 4$ V) the conduction process becomes essentially bulk limited. The symmetry of the characteristics with polarity of voltage bias indicates that the trapping parameters are uniform through the length of the insulator.

All these results are in accordance with the previous SDRC studies.

---

*Work supported in part by National Research Council and Defense Research Council of Canada.

†Now with Precision Electronics Components, Toronto, Canada.

[1]J. G. Simmons, J. Phys. Chem. Solids 32, 1987 (1971).

[2]J. G. Simmons, J. Phys. Chem. Solids 32, 2581 (1971).

[3]J. G. Simmons, Phys. Rev. 166, 912 (1968).

[4]J. G. Simmons and G. S. Nadkarni, J. Vac. Sci. Tech. 6, 12 (1969).

[5]G. S. Nadkarni and J. G. Simmons, J. Appl. Phys. 41, 545 (1970).

[6]G. S. Nadkarni and J. G. Simmons, J. Appl. Phys. 43, 3741 (1972).

[7]G. S. Nadkarni and J. G. Simmons, J. Appl. Phys. 43, 3650 (1972).

[8]J. G. Simmons and G. S. Nadkarni, Phys. Rev. B (to be published).

[9]J. G. Simmons and G. W. Taylor, Phys. Rev. B (to

be published).

[10]In this equation we are making the *a priori* assumption, based on earlier SDRC studies on the samples, Ref. 8, that the trap levels are contained within a narrow band of energy [see Fig. 6(a)] which will be shown to be the case here also. Furthermore, in light of these remarks, it is readily shown that $\psi_m - \psi_i \cong \phi_0 - (E_c - \bar{E}_t)$.

[11]J. G. Simmons and M. C. Tam, second preceding paper, Phys. Rev. 7, 3706 (1973).

[12]Note that this trap depth is not corrected for the Poole–Frenkel effect.

[13]Although this value *per se* is within the experimental error of the measurement of the trap depth, the actual spread of the trap can be determined with a much greater accuracy than the trap depth, by virtue of the fact that we know the exact expression for the It-$\log_{10}t$ characteristic (9) for a discrete trap; hence, any disparity, no matter how small, between the theoretical and experimental characteristics is a measure of the spread of the trap level.

PHYSICAL REVIEW B VOLUME 7, NUMBER 8 15 APRIL 1973

Carrier-Concentration-Dependent Mobility in n-Type High-Purity Germanium*†

James L. Blankenship
Oak Ridge National Laboratory, Oak Ridge, Tennessee 37830
(Received 13 November 1972)

The Hall mobility of electrons in high-purity germanium was studied over a range from 7 to 200 °K in a series of samples both before and after irradiation with ^{60}Co γ rays. In several unirradiated samples the mobility was limited mainly by lattice scattering down to 7 °K. The mobility at 35 °K decreased with radiation dose for all samples, but the magnitude of the decrease was greater in samples having lower carrier concentrations n_e. This decrease was well correlated with n_e. Measured mobilities at 35 °K were significantly lower than values calculated from the Brooks–Herring impurity-scattering expression for $n_e < 10^{12}$ cm^{-3}. At $n_e = 10^{11}$ cm^{-3} the measured mobility was 0.01 times the calculated mobility. No satisfactory explanation has been found.

I. INTRODUCTION

The Hall coefficient and conductivity were studied in γ-irradiated samples cut from a selected special ingot[1] of n-type Ge to determine the carrier concentration and Hall mobility as a function of temperature. Because this newly available material had extremely low net impurity concentrations (10^{11} to 3×10^{12} cm^{-3}), changes in its electrical properties could be detected at much lower radiation doses than had been possible with less pure materials used heretofore in radiation-effects studies.[2] The temperature dependence of carrier concentration was analyzed to measure the donor and acceptor impurity concentrations and the concentration of acceptor states associated with radiation defects. Details of these measurements are reported elsewhere.[3]

In this paper we describe the measured changes in mobility produced by irradiation and compare them with theoretical behavior. Several features of observed reduction in mobility are not explained by the present formulations of scattering rates due to lattice vibration and ionized impurities. Mobility reductions measured at 35 °K show close correlation with carrier concentrations less than 10^{12} cm^{-3} and poor correlation with radiation dose. At lower carrier concentrations, the mobility reduction at 35 °K was up to 100 times greater than the calculated effect of ionized impurity scattering.

II. EXPERIMENTAL DETAILS

All samples used in this study were taken from one ingot, RL-331,[1] which we selected as the purest of 15 ingot specimens examined. The carrier concentration and mobility data taken on samples from this ingot showed nearly ideal temperature functional behavior. Since the material was relatively free of deep traps, the effects of radiation damage could be determined more precisely.

The net donor concentrations varied gradually over an 8-cm distance along the growth axis, from 2×10^{12} cm^{-3} at the lower (tail) end to 5.7×10^{11} cm^{-3} at the upper (seed) end. The total impurity concentration (donors plus acceptors), measured by analyzing the freeze-out of carriers, was between 5.5×10^{12} and 3.5×10^{12} cm^{-3} throughout the ingot segment.

The samples were cut in the shape of a six-arm bridge with four side terminals. Voltages were measured with a digital voltmeter with 10^{12}-Ω input impedance. Magnetic fields between 0.5 and 4.5 kG were used as required. Above 40 °K, temperatures were measured with a Cu-constantan thermocouple; below 40 °K, a Pt or Ge resistance thermometer was used.

A specially designed temperature-control system and sample holder kept the samples in an isothermal environment at constant temperature while the voltages were being measured.